RSC Advances

ROYAL SOCIETY OF CHEMISTRY

www.rsc.org/advances

RSC Advances

RSCPublishing

ARTICLE

Electrically pressure sensitive poly(vinylidene fluoride)/polypyrrole electrospun mats.

Cite this: DOI: 10.1039/x0xx00000x

C. Merlini [a,b], G. M. O. Barra [a], T. Medeiros Araujo [b], A. Pegoretti [b].

Received 00th January 2012,
Accepted 00th January 2012

DOI: 10.1039/x0xx00000x

www.rsc.org/

Non-woven mats with highly pressure-sensitive electrical conductivity has been prepared by electrospinning of poly(vinylidene fluoride) (PVDF) containing up to 23 wt% of polypyrrole (PPy) particles synthesized by using dodecylbenzene sulfonic acid (DBSA) as a dopant. The obtained mats have been characterized by dynamic mechanical thermal analysis, differential scanning calorimetry, thermogravimetric analysis, infrared spectroscopy, scanning electron microscopy and nitrogen adsorption BET. Electrical resistivity changes of PVDF/PPy blends were investigated during loading-unloading compressive cycles. It has been observed that the electrical resistivity varies reversibly with the applied compressive stress. The maximum sensitivity was obtained for a PVDF/PPy blend containing 13 wt% of PPy, manifesting an electrical resistivity drop of 10 orders of magnitude, i.e. from 10^{17} to 10^{7} Ω cm^{-1} upon application of a compressive stress of 5 MPa. This peculiar response can be attributed to the formation of stress-induced conducting pathways in the electrospun network. Considering the remarkable resistivity change and the reproducibility of the phenomenon after repeated loading-unloading cycles, this mat may found application as a pressure sensor.

Introduction

Over the past years the development of electrically conductive polymer composites with properties suitable for pressure sensor applications (e.g. fast and linear response, reproducibility, low cost and high sensitivity) increased exponentially.[1] These pressure sensitive materials have been commonly prepared by addition of conductive fillers, such as conducting polymers,[1,2,3,4,5] carbon black [6,7] carbon particles [8] and graphite [9] to insulating polymeric matrices, like thermoplastic polymers [2,7] or unsaturated rubbers.[6,8] An important requirement for sensing materials in pressure sensor devices is their ability to change the electrical resistivity by compressive applied forces.[10] The electrical response of these materials under loading - unloading cycles depends on various factors, such as the structure, concentration, distribution and dispersion of conductive fillers, chemical interaction between components, physical properties of the polymer matrix, etc... Moreover, the preparation methods and test conditions, including stress levels and temperature values, influence directly the material sensitivity.[1,10]

The effect of a compressive stress on the resistivity of conductive polymeric composites produced from bulk material has been studied by several authors.[1,2,8,10,11] In most cases, electrical resistivity variations between 1 to 5 orders of magnitude have been reported, usually with resistivity values ranging between 10^{3} to 10^{8} Ω cm^{-1}. Additionally, the majority of these pressure sensitive materials display some degree of hysteresis after subsequently compression cycles.[1,2,11] Several strategies have been investigated to improve the sensitivity and reproducibility of these conductive polymeric systems. A possible alternative is the development of polymeric membranes composed of fibers coated by intrinsically conducting polymers (ICP's) such as polypyrrole (PPy) and polyaniline (PANI).[12,13] These materials can be commonly prepared using *in situ* oxidative processes or electrochemical methods in the presence of natural or synthetic insulating polymer fibers. Electromechanical tests showed that ICP´s

coated fibers can be used as pressure-sensitive devices, combining the electrical conductivity with good compression sensitivity for low amounts of conducting polymer.[12]

Another promising alternative is the development of pressure sensing devices using nano-structured materials.[14] The electrospinning technique can be used to produce polymeric nano-fiber mats, leading to the possibility of obtaining new nanostructured composites with an improved sensitivity and faster response. In fact, advantages can be offered by their very large surface area to volume ratio (up to 10^3 times larger in comparison to micro-fibers),[15] high density of sensitive sites and porous structure, associated with the properties of conductive polymers.[16,17,18,19] In the electrospinning process, an elevated electric field (of about 1 kV cm^{-1}) is applied to a needle through which a polymer solution is delivered. When the applied electric field overcomes the surface tension and the viscoelastic forces in the droplet, a charged jet of the polymer solution is ejected. While traveling to the collector, the jet exhibits bending instabilities, the solvent evaporates and solidified fibers are deposited on a collector.[15,20] Conductive sub-micron fiber mats can be produced by i) direct electrospinning technique, in which fibers are electrospun from a mixture containing an insulating polymer and ICP dispersed in a common solvent[17,19,21,22,23] or by ii) an indirect method, in which the insulating fibrous membrane is firstly prepared by electrospinning and after coated with PPy or PANI through pyrrole or aniline oxidative polymerization.[18,24,25,26]

In this context, poly(vinylidene fluoride) (PVDF) is a suitable polymer matrix to prepare electrospun conductive polymer composites due to its unique pyroelectric/piezoelectric features, coupled with superior mechanical properties and easy processability.[16] Highly sensitive piezoelectric sensors based on PVDF films and nanofibers have been successfully obtained and described by several authors.[27,28,29,30,31] These materials are commonly used in piezoelectric devices in order to measure forces and strains, at a micron-scale in terms of displacement, especially those of dynamic nature, such as vibrations, accelerations and oscillations [14]. Such devices present high sensitivity in the low-pressure regime (□10 kPa). However, to the best of our knowledge, there are no studies published in the open scientific literature concerning the development of electrospun conductive mats based on PVDF/PPy for pressure sensors applications. The PVDF/PPy mats developed in the present study can be employed in a sensor capable to generate an outstanding variation of the electrical resistivity at high-pressure levels (1-5 MPa). Unlike the PVDF sensors, that are based on the piezoelectric concept, the PPy particles inside of the PVDF fibers may form a conducting network under pressure, according with a percolative theory. Additionally, the use of these materials with sensitivity at high pressure avoid signal shift due to undesirable noise and/or interference, such as mechanical vibrations or thermal expansion .[27].

Therefore, the focus of this study is on the preparation of conductive sub-micron PVDF/PPy fiber mats through electrospinning technique and on the investigation of their microstructure, termomechanical properties and stress-dependent conductivity under cyclic loads.

Experimental

Materials

Pyrrole (Aldrich; 98%) was distilled under vacuum and stored in a refrigerator. Iron (III) chloride hexahydrate ($FeCl_3.6H_2O$) (analytical grade, Aldrich Chemistry). Dodecylbenzenesulfonic acid (DBSA), 70 wt% solution in 2-propanol and poly(vinylidene fluoride) (PVDF) with molecular weight (M_w) of 534.000 g mol^{-1} were supplied by Aldrich Chemistry. Dymethylformamide (DMF) (99.8%) and acetone (99.5%) were purchased from Aldrich and Merck, respectively. With exception of the pyrrole, all materials were used without further purification.

Polypirrole synthesis

The pyrrole oxidative polymerization was performed in the presence of dodecylbenzenesulfonic acid (DBSA) using ferric chloride ($FeCl_3$) as oxidant, according to [32] Firstly, the anionic surfactant DBSA (1.88 g) was dissolved in 0.05 L of distilled water and then 2 mL (0.3 mol L^{-1}) of pyrrole (Py) was added. After 10 minutes, 16.2 g of Iron (III) chloride hexahydratate ($FeCl_3.6H_2O$) dissolved in 0.05 L distilled water was slowly added. The oxidant-to-monomer molar ratio was 2/1. The polymerization was carried out for 6 hours at room temperature under magnetic stirring. The precipitated PPy particles were filtered and thoroughly washed with distilled water in order to extract the byproducts and residues of the reaction and vacuum dried at room temperature.

Preparation of PVDF/PPy fiber mats by electrospinning

PVDF was dissolved in DMF under stirring for 2 hours at 70 ºC resulting in a 20 wt% solution. After cooling, acetone was added to the solution under stirring in a DMF/acetone proportion of 75/25 by weight, according to [33] PPy particles were inserted into the PVDF solution at various weight concentrations (up to 23 wt%). The suspensions were mechanically stirred for 10 minutes, and sonicated with an ultrasonic probe (Ultrasonic Processor UP400S Hielscher, 50 W and 60 Hz) for 5 minutes. The suspensions were spun through a 5 mL syringe (needle with an internal diameter of 2.6 mm) coupled with a syringe pump (Harvard Apparatus 11 Plus) at a flow rate of 1.0 mL h^{-1}. An electric field was generated using a high voltage supply (Spellman SL30), which generates DC fields up to 30 kV. The positive pole was connected to the syringe needle and the collector plate was grounded. PVDF/PPy fiber mats were obtained using voltage between 15 and 23 kV and needle-to-collector distance of 30 cm. All the electrospinning process was performed at 25 ºC and humidity of 60 % and the fibers were collected on an aluminum foil. The

samples have been denoted as PVDF/PPy_x, where x represents the weight content of PPy in the blend.

Characterization techniques

An elemental analysis (carbon, hydrogen and nitrogen) was performed with a Perkin-Elmer CHN 2400 analyzer. The combustion process was held at 925 °C using pure oxygen (99.995 %).

The specific surface area (SSA) of the electrospun samples was determined by nitrogen adsorption BET method (ASAP 2010, Micromeritics, USA).

The viscosity of the solutions was evaluated at 25 °C using a Brookfield viscometer Model RVT 90658 using SC4-21 spindles. The shear rate was fixed at 0.46 s^{-1}.

Attenuated-total-reflectance Fourier-transform-infrared (ATR-FTIR) spectroscopy was performed on a Bruker spectrometer, model TENSOR 27, in the range of 4000 - 400 cm^{-1} by accumulating 32 scans at a resolution of 4 cm^{-1}.

The microstructure of electrospun mats of neat PVDF and PVDF/PPy blends was analyzed by a Zeiss - Supra 60 field emission scanning electron microscope (FESEM), and by a Jeol JSM-6390LV scanning electron microscope (SEM).. The samples were sputtered with gold and observed using a secondary electron detector and applied tension between 2 and 4 kV.

Thermogravimetric analysis (TGA) was carried out using a TGA Q5000IR (TA Instruments, USA) thermo-gravimetric analyzer. The analyses were performed at 10 ºC min^{-1} from 35 ºC to 700 ºC under a nitrogen flux of 25 mL min^{-1}.

Differential scanning calorimetry (DSC) measurements were performed on a Mettler DSC30-TA Low Temperature and a Metler TC 15 TA Controller at a heating rate of 10 ºC min^{-1}, from -75 ºC to 220 ºC, under a nitrogen flux of 100 mL min^{-1}.

The cristallinity content (*Xc*) of PVDF was calculated on the basis of Equation 1.

$$Xc = \frac{\Delta H_f}{\Delta H_f^* \varphi}.100 \quad (1)$$

Where ΔH_f is the sample enthalpy of fusion, ΔH_f^* is the heat of fusion of perfectly crystalline PVDF (104.7 J g^{-1})[34] and □ is the weight fraction of PVDF in the PVDF/PPy blends.

Dynamic mechanical thermal analysis (DMTA) experiments were carried on a DMA Q800 (TA Instruments) under the tensile mode on rectangular specimens with a width of 6.4 mm and a length of 30 mm. The analyses were performed at a frequency of 1 Hz, from -100 to 130 ºC, at a heating rate of 3 ºC min^{-1} and a peak-to-peak displacement of 64 μm.

The transmission electron microscope (TEM) experiments were performed on a JEM-1011 microscope with an acceleration voltage of 100 kV.

The setup used to evaluate the electrical-mechanical response of the PVDF/PPy blends consists in an universal testing machine (Instron, Model 5969) to apply a controlled stress and an electrometer (Keithley 6517A) to acquire the resistivity data, using a software developed exclusively for this work. The interface RJ45 and GPIB were used to connect the Instron and electrometer to the computer, respectively. The specimen was placed between two electrodes (Ø = 22.5 mm) which were confined in cylinder made of poly(tetrafluoroethylene) in order to electrically isolate the sample from the mechanical testing fixtures. The device was then placed between the testing plates of the universal testing machine. The electrodes were connected to the electrometer for measuring the volume resistivity of the blends during loading and unloading. The samples were loaded up to 5 MPa at a loading rate of 1 MPa min^{-1}, the compressive stress was then released at the same rate. For each sample, loading-unloading sequences of 5 and 25 cycles were performed on different specimens. The electrical resistivity (ρ) value (in Ω cm^{-1}) were calculated through Equation 2, where *R* is the measured resistance (Ω), *d* is the sample diameter (cm) and *w* is the specimen thickness (cm).

$$\rho = \frac{\pi . R . d^2}{4w} \quad (2)$$

Results and Discussion

PVDF/PPy fiber mats were prepared through electrospinning from PVDF solutions containing various fractions of PPy particles. The apparent viscosity of the starting solutions, the PPy content in each blend, the electrical resistivity, the surface area and the fiber diameter of electrospun PVDF and PVDF/PPy mats are reported in Table 1. Considering that nitrogen is absent in the PVDF structure, the PPy effective amount in the blends can be determined by CHN elemental analysis from the difference in nitrogen content between the pure PPy and the blends. The PPy amount on the PVDF/PPy electrospun blends increases significantly with increasing polypyrrole concentration in the starting solution, with values of 5.11, 13.61 and 26.90 wt% for the electrospun mats obtained from solutions with 3, 13 and 23 wt% of PPy, respectively. The real amount of PPy in the electrospun PVDF/PPy fibers is very close to the amount of PPy in the starting solutions, thus confirming a homogeneous dispersion of the PPy in the suspension and its transfer in the electrospun mats. The synthesized PPy displays an electrical resistivity of 0.36 ± 0.3 Ω cm^{-1} while PVDF and PVDF/PPy electrospun mats behave as insulating materials with electrical resistivity values higher than 10^{14} Ω cm^{-1}. This indicates that the electrical percolation threshold is not reached even if a PPy content of 23 wt% is introduced in the PVDF matrix. On the other hand, blends containing more than 23 wt% of PPy are not suitable for the electrospinning technique due to their very high apparent viscosity. It is interesting to observe that the specific surface area of PVDF/PPy electrospun mats increases as the PPy content in the blend increases, with values ranging from 7.59 m^2 g^{-1} for neat PVDF to 22.16 m^2 g^{-1} for PVDF/PPy blends

containing 23 wt% of PPy. This trend is related to the observed decrease of the fiber diameter on the PVDF/PPy electrospun mats as the PPy content increases.

Nominal PPy content in the blend (wt%)	Measured PPy content in the blend (wt%)*	Apparent viscosity (mPa s)	Electrical resistivity $x10^{14}$(Ω cm^{-1})	Specific surface area (m^2 g^{-1})	Fiber diameter (nm)
0	0	2476	27.00 ± 1.20	7.59 ± 0.05	854 ± 271
3	5.11 ± 0.07	2485	24.10 ± 3.40	6.65 ± 0.08	968 ± 280
13	13.61 ± 0.22	6520	1.39 ± 1.31	15.88 ± 0.39	790 ± 170
23	26.90 ± 0.44	48830	1.60 ± 1.27	22.16 ± 0.33	460 ± 90

* from CHN elemental analysis

Table 1. Measured content of PPy in the PVDF/PPy electrospun mats, apparent viscosity of the starting solutions, electrical resistivity, surface area and fiber diameter of electrospun mats.

Figure 1(a-d) illustrates FESEM images of electrospun mats of neat PVDF and PVDF/PPy blends containing various amounts of PPy. Micrographs show that both PVDF (Figure 1a) and PVDF/PPy mats (Figure 1b and 1c) are constituted by a three-dimensional fibrous network. Neat PVDF fiber mats displays an average diameter of 854 ± 271 nm. It is worthwhile to note that the average diameter of PVDF/PPy electrospun mats decreases as the PPy content in the blend increases, with an average value of 460 ± 90 nm for the PVDF/PPy_23 specimen. The addition of PPy induces a modification of the properties of the solutions, such as viscosity and electrical conductivity. As a consequence, the voltage applied during the electrospinning process has to be adjusted, from 15 to 23 kV with the increasing of PPy content. One of the effects of increasing the voltage is the reduction of the fiber diameter wich can be observed as the amount of PPy increases. As the amount of PPy is increased from 3 to 13 wt% the formation of PPy agglomerates along the electrospun fibers can be noticed, even if no presence of PPy particles outside the electrospun fibers can be observed. A non-woven structure with the existence of larger agglomerates along the fibers is formed in the blends containing 23 wt% of PPy. Nevertheless, the micrographs of the last one revealed an incidence of a consistent quantity of PVDF/PPy agglomerates outside of the non-woven structure. The importance of this peculiar microstructure to reach a stress-induced electrical conductivity will be further discussed.

RSC Advances RSCPublishing

ARTICLE

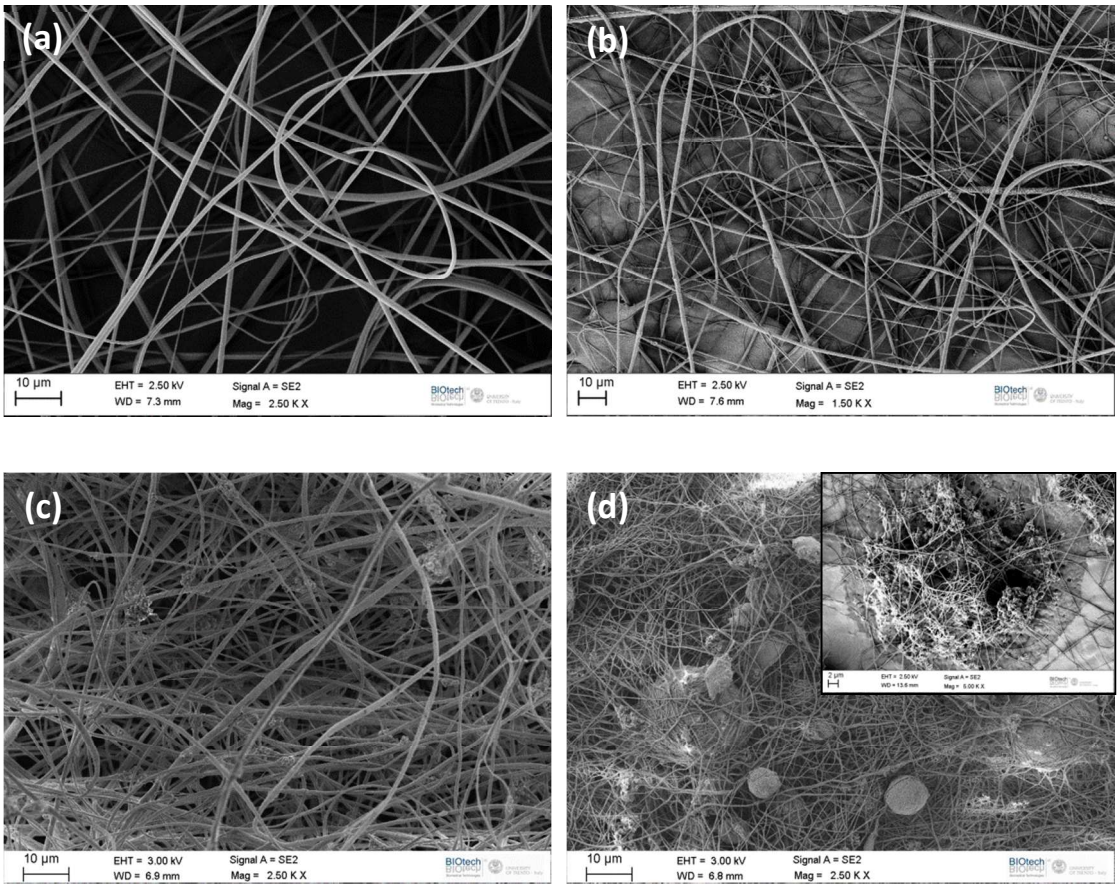

Figure 1. FESEM micrographs of electrospun mats of (a) neat PVDF, (b) PVDF/PPy_3, (c) PVDF/PPy_13 and (d) PVDF/PPy_23.

FTIR spectra of PPy, PVDF and PVDF/PPy fiber mats are reported in Figure 2. The spectrum of PPy exhibits absorption bands at 1520 cm^{-1} and 1424 cm^{-1}, assigned to C–C and C–N stretching vibration of pyrrole ring, respectively.[11,35] The absorption band at 1275 cm^{-1} is assigned to C–H or C–N in-plane deformation modes,[36] while the bands at 1121 and 1015 cm^{-1} are assigned to the C–H bending modes. The band centered at 960 cm^{-1} is related to the C–H out-of-plane deformation of pyrole ring.[11,35] An interesting feature of PVDF is its polymorphism, i.e. the possibility to form different crystalline structures, such as, alpha (α), beta (β), gamma (γ) and delta (δ), depending on the crystallization conditions.[37] The various PVDF phases can be identified by the absorption bands in the FTIR spectrum. Electrospun PVDF spectrum shows absorption bands at 1402 and 876 cm^{-1} (band for amorphous phase) attributed to the C–F stretching vibration and at 1172 cm^{-1} assigned to the C–C bond.[24,37,38,39] The bands at 837, 1073 and 1274 cm^{-1} are associated with the β phase.[34,39,40,41] The bands at 603 and 1232 cm^{-1}, are characteristics of α and γ phases, respectively.[39] The FTIR spectra of PVDF/PPy blends show absorption bands similar to those of neat PVDF, however, the blend with 23 wt% of PPy presents a stronger band at 1540 cm^{-1}. This behavior can be related to the presence of PVDF/PPy agglomerates outside of the fibers, as observed in the FESEM micrographs. The electrospun fibers mats spectrum shows predominance of β phase, which offers the highest piezo-, pyro- and ferro-electric properties and it is particularly interesting for sensing applications.[33] This result suggests that electrospinning process could have induced the formation of the β phase in the PVDF fibers mats.[40,41]

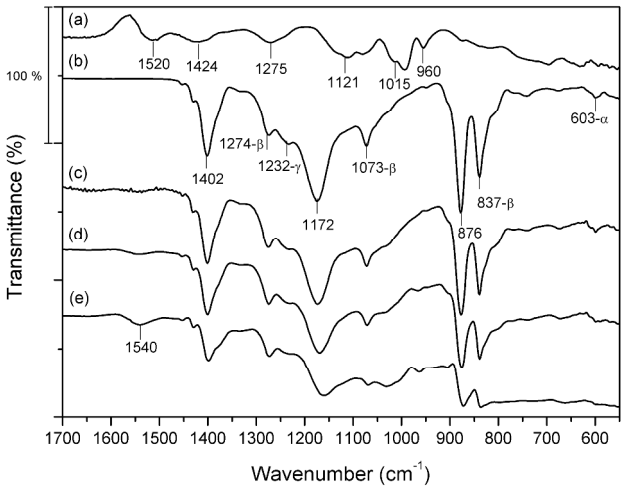

Figure 2. FTIR spectra of (a) PPy particles, (b) electrospun PVDF, (b) PVDF/PPy_3, (c) PVDF/PPy_13 and (d) PVDF/PPy_23.

The thermogravimetric curves of PPy particles and of electrospun mats of neat PVDF and PVDF/PPy blends are reported in Figure 3. PPy particles present a main weight loss starting from 320 ºC, which corresponds to the polymer chain degradation. On the other hand, PVDF shows weight loss at 473 ºC which is attributed to the polymeric chain decompositions, with 5.50% of residue at 700 ºC.[42] The PVDF/PPy blends prepared with various amounts of PPy start to decompose at temperatures higher than that of pure PVDF and showed a single weight loss attributed to the thermal decomposition of both components. As a result, the maximum decomposition temperature shifts to higher values with increasing PPy concentration. This behavior can be attributed to the site-specific interaction between PPy and PVDF groups. Moreover, at 700 ºC the residue obtained for the PVDF/PPy blends was higher than pure PVDF due to the presence of PPy and changes accordingly with PPy concentration in the blends.

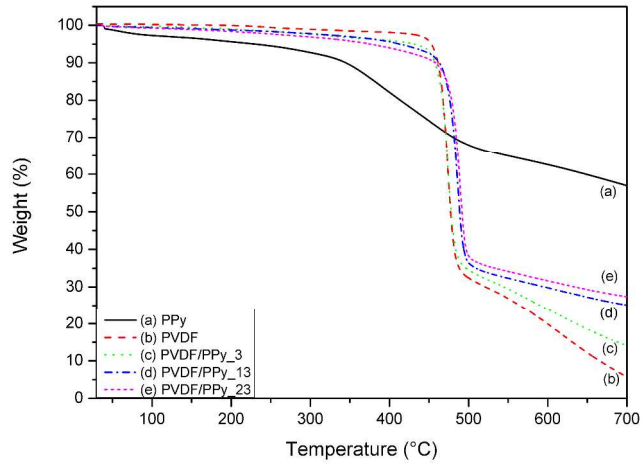

Figure 3. TGA curves of (a) PPy particles, and electrospun (b) PVDF, (c) PVDF/PPy_3, (d) PVDF/PPy_13 and (e) PVDF/PPy_23 mats.

Figure 4 shows the DSC thermogram of electrospun mats of PVDF and PVDF/PPy blends with various PPy weight fractions. An endothermic peak at 54 ºC can be clearly detected on the thermogram of pure PVDF. This peak, which disappears in the immediate second heating run, has been already reported for PVDF with various possible origins: upper glass transition [43], reorganization within conformationally disordered α-crystals [44], molecular motions corresponding to an α_c relaxation in the crystalline/amorphous interface [45], melting of paracrystalline domains [46]. More recently, further insights on the nature of this annealing peak has been provided by Neidhöfer et al. [47]. An endothermic transition at 157.9 ºC is assigned to the melting of α-form crystalline structure while the second endothermic peak at 167.9 ºC can be related to the *β*-form of PVDF crystals. According to the literature,[48,49] double melting transitions are frequently observed in PVDF due to its polymorphic structure. This behavior can be associated to the fact that the high electrical field and mechanical stretching typical of the electrospinning process can induce the formation of piezoelectric β-phases in electrospun PVDF fibers.[50] For the electrospun PVDF/PPy blends obtained with different PPy content, the endothermic transition associated with α or α_c phases is observed at around 60 ºC and the melting temperature is located, at 158.8, 159.6 and 161.6 ºC for blends containing 3, 13 and 23 wt% of PPy, respectively.

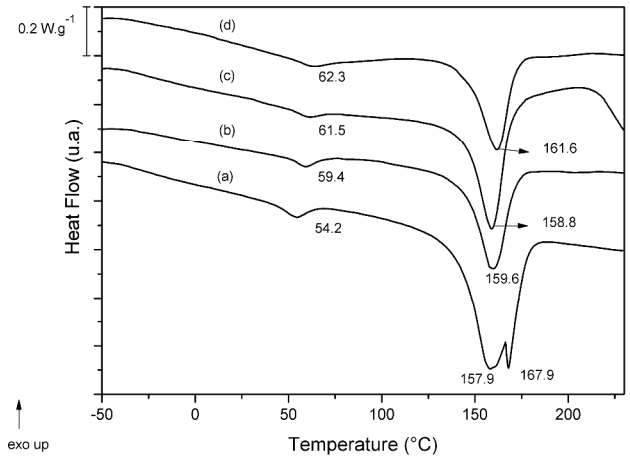

Figure 4. DSC curves of electrospun (a) PVDF, (b) PVDF/PPy_3, (c) PVDF/PPy_13 and (d) PVDF/PPy_23 mats.

Table 2 shows the melting temperature (T_m), the sample enthalpy of fusion (ΔH_f) and the crystallinity (X_c) of electrospun PVDF and PVDF/PPy blends. It is worthwhile to note that neat PVDF displays a crystallinity degree higher than other values reported in the literature for PVDF electrospun mats.[38,40] Additionally, the PVDF crystallinity is higher than electrospun PVDF/PPy blends, thus indicating that the addition of PPy particles can hinder the crystallization of PVDF chains.[42]

RSC Advances RSCPublishing

ARTICLE

Sample	ΔH_f (J g^{-1})	X_c (%)	*Melting temperature (T_m)* (°C)
PVDF	82.9	79.0	157.9 and 167.9
PVDF/PPy_3	48.8	49.0	158.8
PVDF/PPy_13	61.7	59.0	159.6
PVDF/PPy_23	42.4	55.4	161.6

Table 2. Melting enthalpy (ΔH_f), crystallinity (X_c) and melting temperature (T_m) of the electrospun PVDF and PVDF/PPy blends.

Storage modulus (E') as a function of temperature for electrospun mats of neat PVDF and PVDF/PPy blends is reported in Figure 5(a). Over the entire temperature range, E' values of neat PVDF are higher than those found for the blends over the whole temperature range. In addition, the storage modulus of the blends decreases abruptly when the PPy content increases. This effect can be attributed to the lower crystallinity of the PVDF/PPy blends and the presence of PPy in the electrospun mats which reduces the intermolecular dipole bonding of PVDF fibers, and hence, reducing the Young modulus.

Loss tangent (tanδ) thermograms for electrospun mats of neat PVDF and PVDF/PPy blends are reported in Figure 5(b). The two transition temperatures at around -42 °C and 86 °C, corresponds to the glass transition and relaxation process associated with molecular motions of crystalline fraction, respectively, and are affected by the presence of PPy, with exception of the blend containing 23 wt% of PPy.[51,52] The shift of T_g to higher temperatures can be tentatively explained by considering the decrease in the mobility of the PVDF chains due to the presence of PPy.[53] Moreover, the intensity of the peak corresponding to the glass transition temperature reduces significantly as the amount of conducting polymer in the blend increases. However, the tanδ intensity and T_g of PVDF/PPy blends with 23 wt% are quite similar of those for pure PVDF mats. This behavior can be related to the presence of PPy particles or agglomerates, located almost exclusively outside the electrospun fibers.

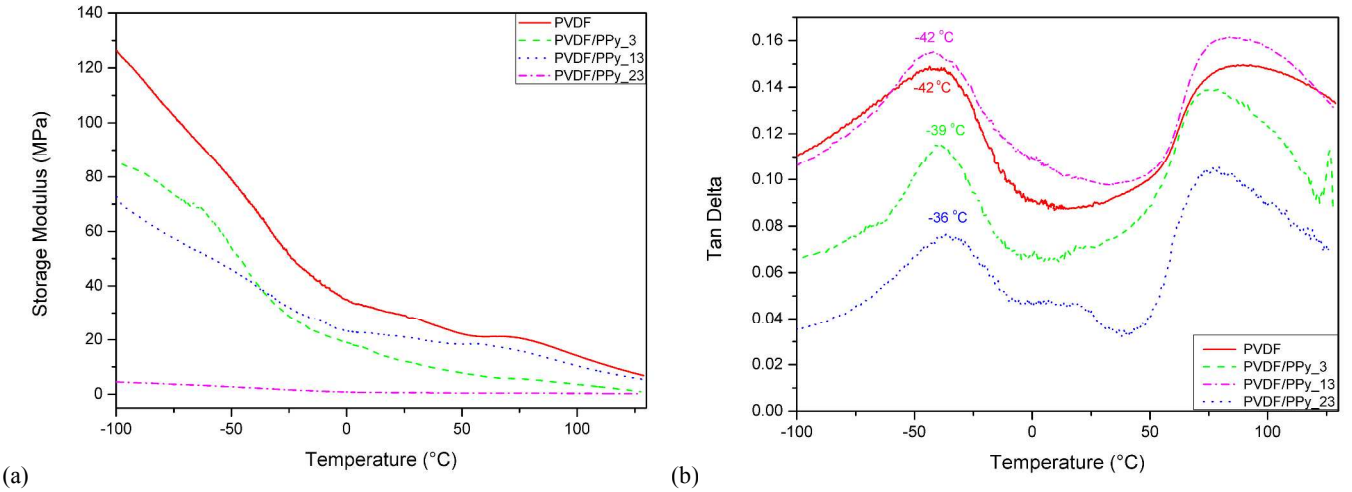

(a) (b)

Figure 5. DMTA traces (a) storage modulus and (b) loss factor of electrospun mats of neat PVDF and PVDF/PPy blends.

Figure 6(a-c) shows the variation of the electrical resistivity of PVDF and PVDF/PPy electrospun mats subjected to 25 consecutive compressive loading-unloading stress cycles. As expected, neat PVDF does not display a significant change of the electrical resistivity when the compressive stress is applied, since that piezoelectric materials it is not the resistance which is expected to change but the polarization charges and the induced voltage. On the other hand, the compressive stress has a remarkable effect on the electrical resistivity of the blends. When the system is subjected to a compressive stress (loading cycle), the resistivity value decreases several orders of magnitude as the pressure increases. Moreover, it is interesting

to note that the initial resistivity value is almost completely recovered when the applied stress is removed. The minimum pressure value which the PVDF/PPy mats display detectable variation on the electrical resistivity is around 0.05 MPa, since the electrical resistivity reduces almost one order of magnitude. It is worthwhile to note that the PVDF/PPy blends with 3 and 13 wt% of PPy exhibit very wide electrical resistivity changes (ranging from 10^{16} down to 10^{8} Ω cm^{-1} and from 10^{17} down to 10^{7} Ω cm^{-1}, respectively), with reproducible response after 25 cycles. The sensitivity, i.e. variation on the electrical resistivity with the compression stresses, is much higher than the ones reported in the open scientific literature for conventional systems based on conducting polymers.[1,2,3,4,5] However, when the conductive filler content is increased to 23 wt%, the response is markedly different. In fact, the electrical resistivity changes from 10^{14} up to 10^{7} Ω cm^{-1} in the first compressive ramp, due to the arrangements of fibers. However, after unloading and during the subsequent cycles, the electrical resistivity variation is limited to one order of magnitude. This behavior could be attributed to the high amount of PVDF/PPy agglomerates outside the electrospun fibers, as shown in FESEM images (Figure 2d). After the first loading cycle the PVDF/PPy agglomerates touch each other, creating a preferential conductive pathway and consequently reducing the resistivity of the material. Since the agglomerates are not inside the fibers they cannot take advantage of the elastic recovery of the electrospun polymer network after load removal. Increasing the number of loading-unloading stress cycles the PVDF/PPy_23 sample presents a reduction in the variation magnitude of electrical resistivity due to the irreversible deformation.

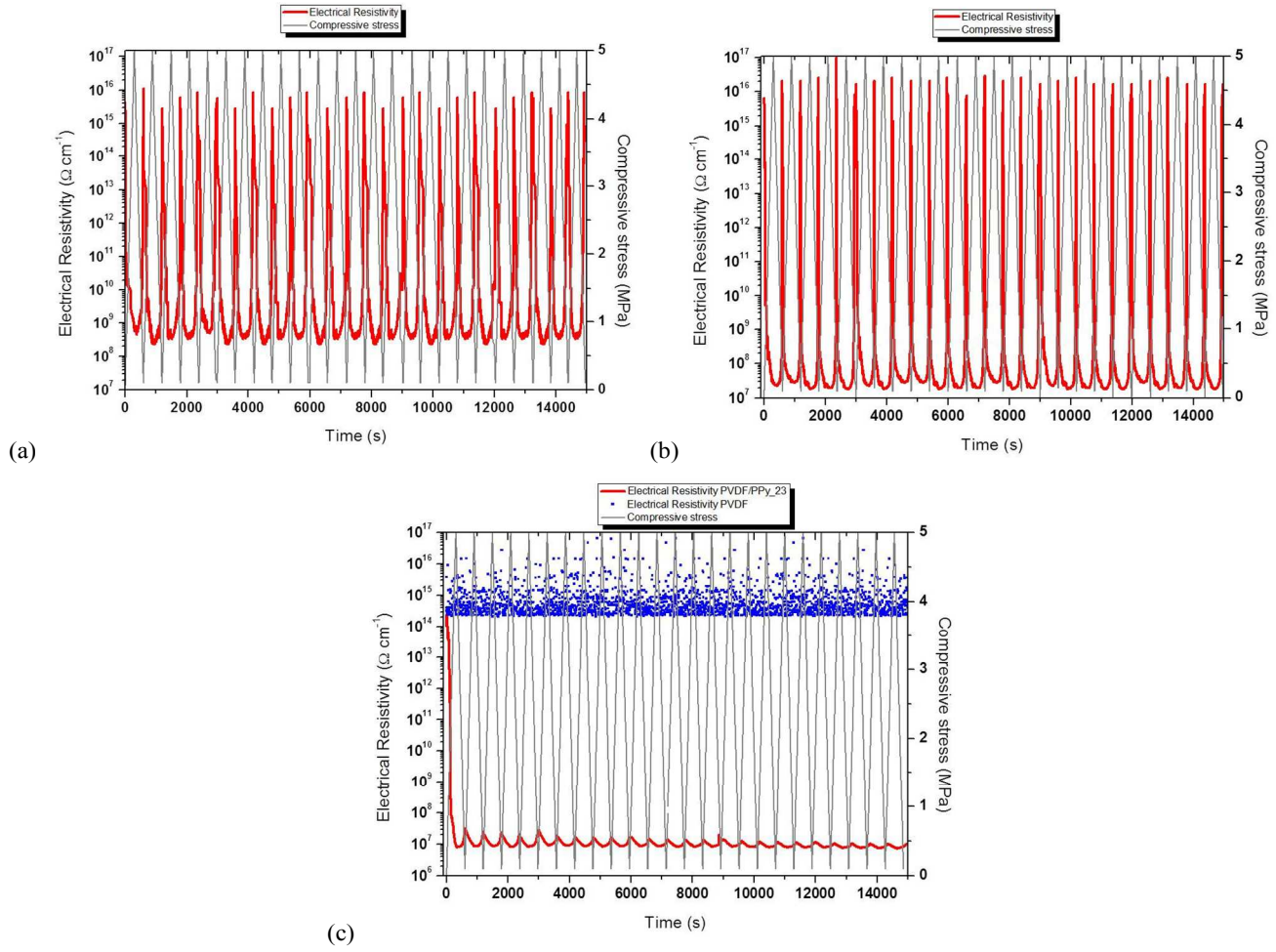

Figure 6. Electrical resistivity as a function of compressive loading-unloading stress cycles on electrospun mats of (a) PVDF/PPy_3, (b) PVDF/PPy_13, and (c) PVDF/PPy_23. On the plot (c) the behavior of a neat PVDF electrospun mat is also reported.

As schematized in Figure 7 the PVDF/PPy electrospun mats can be represented as a three-dimensional fiber network structure with randomly distributed fibers, with PPy particles located inside the fibers for blends containing up to 13 wt% of PPy. The microstructure was confirmed by TEM micrograph of fiber of PVDF/PPy_13, as showed in Figure 7. TEM analysis indicated the presence of PPy particles embedded in the PVDF matrix. In this case, the average inter-fiber gap allows only relatively few contacts between the fibers and limited conducting pathways. Consequently, the electrical resistivity of

the mat is high, with values quite similar to that of neat PVDF mat. Under compressive stress the inter-fiber gap is reduced, the contacts between fibers may form a conducting pathway. Moreover, the applied compressive stress can reduce the distance between the PPy particles inside the fibers, thus decreasing the electrical resistivity of the blends. Both phenomena are responsible for the large and reversible variations of the electrical resistivity observed of the electrospun blends under compressive stress.

Figure 8a shows the dependence of the electrical conductivity on compressive stress during 25 consecutive loading - unloading cycles performed on the electrospun blend with a PPy content of 13 wt%. This blend composition was selected for a deeper analysis due to its higher sensitivity when compared with the others PVDF/PPy compositions investigated in this work. It is worthwhile to note that the loading-unloading process induce a very reproducible response which is not significantly affected by increasing the number of cycles. This behavior indicates a reversible organization of the fibers in the electrospun mat and, consequently, a restoration of the conducting pathway due to the absence of plastic deformation.

Figure 7. Illustrative scheme of the conducting pathway formation in electrospun conductive polymer blend without pressure and after applying an external pressure. TEM of PVDF/PPy_13 is also reported.

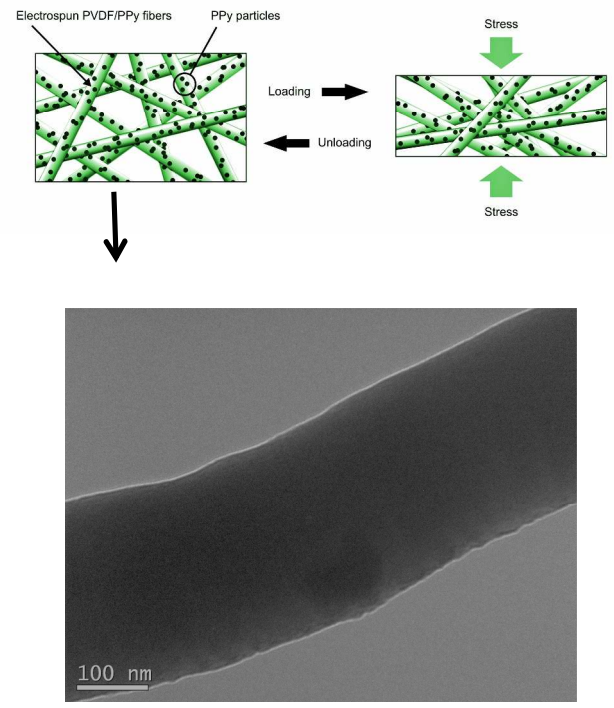

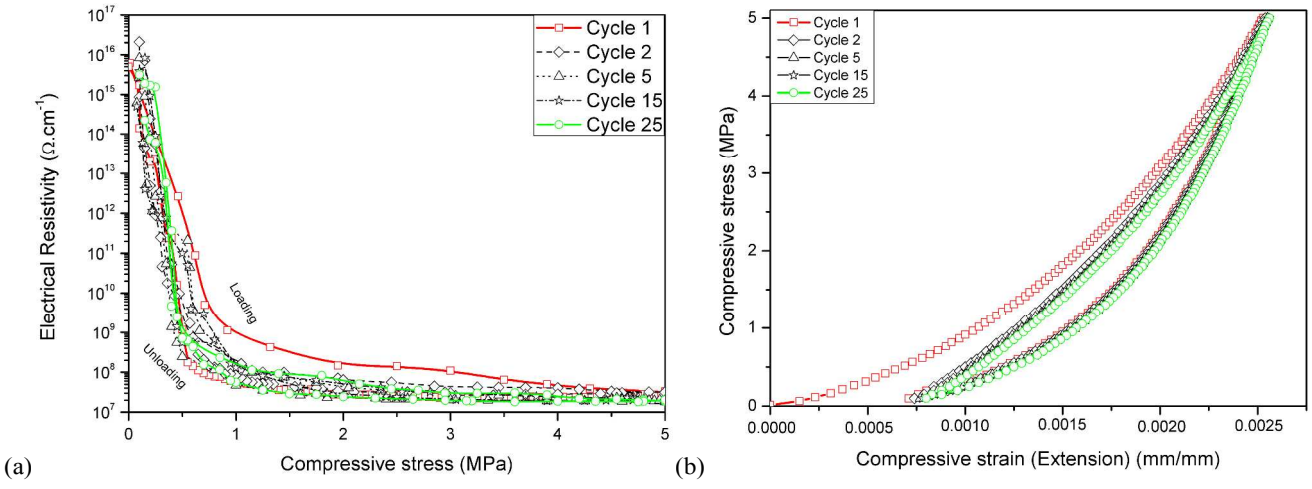

Figure 8. (a) Electrical resistivity as function of compressive stress during 25 loading and unloading cycles (b) Compressive stress as function of compressive strain during 25 cycles. Data referred to the electrospun PVDF/PPy_13 sample.

Figure 8b shows the hysteresis effect on the stress-strain curves when the PVDF/PPy_13 electrospun mat was subject to 25 consecutive loading/unloading cycles. A residual irreversible strain can be observed on unloading after the first loading step probably related to the sample accommodation between the electrodes. However, from the 2nd to 25th cycle no variations of the hysteresis loops can be observed, thus excluding the presence of irreversible phenomena (such as plastic deformation) on the sample. The sensibility of the sensor can be quantified by its response (e.g. voltage, resistivity) over the stress applied. The sensibility of the PVDF/PPy_13 mats varies from 20 to 200 $\Omega.cm^{-1}/Pa$, which is considerably higher than the one found for piezoelectric systems based on neat PVDF fibers (1.0 - 1.66 x 10^{-3} $V.cm^{-1}/Pa$).[27] However it is important to note that the pressure sensor based on a PVDF/PPy mats is designed to work under pressures greater than 0.02 MPa to 5

MPa, while piezoelectric sensor based on PVDF is sensitive in the range from 0.1 Pa to 12 Pa.

SEM micrographs were performed in the PVDF/PPy_13 after 5 and 25 cycles and reported in Figure 9. Electron microscopy does not reveal differences in the morphology of the electrospun fibers before and after the compressive tests, which means that there are no plastic deformation phenomena within the 25 loading-unloading cycles. This observation support the mechanical results presented in figure 8(b), confirming the reversibility of the sensor microstructure upon repeated loading-unloading cycles.

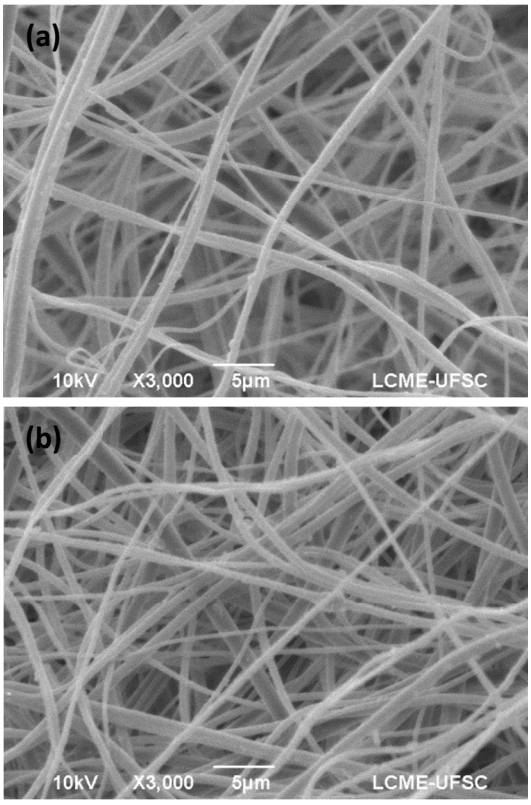

Figure 9. SEM micrographs of electrospun mats of PVDF/PPy_13 after (a) 5 and (b) 25 consecutive compressive loading-unloading stress cycles.

Conclusions

A new pressure sensitivity electrospun polymer mats was successfully obtained through electrospinning of PVDF/PPy blends. Neat PVDF and PVDF/PPy mats displayed high surface area and the presence of β-piezoelectric phase. In the undeformed state, all the investigated electrospun blends behave as insulating materials with resistivity values similar to that of the PVDF matrix. However, under loading and unloading pressure cycles, the blends show a notable variation of several orders of magnitude in the electrical resistivity, which is not observed on the neat PVDF. The electromechanical response is dependent on the amount of PPy particles present in the blend. Furthermore, among the studied compositions, PVDF/PPy blends prepared with 13 wt% of PPy particles show the highest sensitivity, with a variation of electrical resistivity of about 10 orders of magnitude. To the best of our knowledge, the observed electrical resistivity variation is higher than the values reported in the open scientific literature for polymer-based systems. The FESEM micrographs showed that electrospun mats are constituted of fibrous network structure with randomly oriented fibers that under pressure are forced to touch each other, reducing the distance between PVDF/PPy fibers and forming new conducting pathways, consequently decreasing it electrical resistivity. It was also observed that the electrical resistivity response is highly reproducible after repeated loading-unloading cycles.

Acknowledgements

CM gratefully acknowledges the financial support by Conselho Nacional de Desenvolvimento Científico e Tecnológico – CNPq through the program "Science Without Borders", Coordenação de Aperfeiçoamento de Pessoal de Ensino Superior – CAPES and Fundação de Amparo à Pesquisa e Inovação do Estado de Santa Catarina - FAPESC.

Notes and references

[a] Mechanical Engineering Department, Federal University of Santa Catarina (UFSC), Florianopolis, SC, Brazil.
[b] Department of Industrial Engineering, University of Trento, 38123 TN, Italy.

1 Souza, F. G., R. C. Michel and B. G. Soares, *A methodology for studying the dependence of electrical resistivity with pressure in conducting composites*. Polymer Testing, **2005**, 24: p. 998.
2 Barra, G. M. O., R. R. Matins, K. A. Kafer, R. Paniago, C. T. Vasques and A. T. N. Pires, *Thermoplastic elastomer/polyaniline blends: Evaluation of mechanical and electromechanical properties*. Polymer Testing, **2008**, 27: p. 886.
3 Pyo, M. and J.-H. Hwang, *Conductivity changes of dodecylbezensulfonic acid-doped polyaniline during pressure loading/unloading*. Synthetic Metals, **2009**, 159: p. 700.
4 Brady, S., D. Diamond and K.-T. Lau, *Inherently conducting polymer modified polyurethane smart foam for pressure sensing*. Sensors and Actuators A: Physical, **2005**, 119: p. 398.
5 Radhakrishnan, S. and S. B. Kar, *Role of non-linear processes in conducting polymer blends for piezo-sensors Part 2: Studies on polyaniline/SBS blends*. Sensors and Actuators a-Physical, **2005**, 120: p. 474.
6 Job, A. E., F. A. Oliveira, N. Alves, J. A. Giacometti and L. H. C. Mattoso, *Conductive composites of natural rubber and carbon black for pressure sensors*. Synthetic Metals, **2003**, 135-136: p. 99.
7 Knite, M., V. Teteris, A. Kiploka and J. Kaupuzs, *Polyisoprene-carbon black nanocomposites as tensile strain and pressure sensor materials*. Sensors and Actuators A: Physical, **2004**, 110: p. 142.
8 Hussain, M., Y.-H. Choa and K. Niihara, *Fabrication process and electrical behavior of novel pressure-sensitive composites*. Composites Part A: Applied Science and Manufacturing, **2001**, 32: p. 1689.

9 Beruto, D. T., M. Capurro and G. Marro, *Piezoresistance behavior of silicone–graphite composites in the proximity of the electric percolation threshold*. Sensors and Actuators A: Physical, **2005**, 117: p. 301.
10 Sau, K. P., T. K. Chaki and D. Khastgir, *The Effect of Compressive Strain and Stress on Electrical Conductivity of Conductive Rubber Composites*. Rubber Chemistry and Technology, **2000**, 73: p. 310.
11 Merlini, C., B. S. Rosa, D. Müller, L. G. Ecco, S. D. A. S. Ramôa and G. M. O. Barra, *Polypyrrole nanoparticles coated amorphous short silica fibers: Synthesis and characterization*. Polymer Testing, **2012**, 31: p. 971.
12 Souza, F. G., G. E. Oliveira, C. H. M. Rodrigues, B. G. Soares, M. Nele and J. C. Pinto, *Natural Brazilian Amazonic (Curauá) Fibers Modified with Polyaniline Nanoparticles*. Macromolecular Materials and Engineering, **2009**, 294: p. 484.
13 Fernando G. de Souza Jr, L. O. P., Ricardo C. Michel, Geiza E. de Oliveira, *Coconut fibers modified with polyaniline nanoparticles are used in pressure sensor*. Polímeros, **2011**, 21: p.
14 Cullinan, M. A., R. M. Panas, C. M. DiBiasio and M. L. Culpepper, *Scaling electromechanical sensors down to the nanoscale*. Sensors and Actuators a-Physical, **2012**, 187: p. 162.
15 Medeiros Araujo, T., S. Sinha-Ray, A. Pegoretti and A. L. Yarin, *Electrospinning of a blend of a liquid crystalline polymer with poly(ethylene oxide): Vectran nanofiber mats and their mechanical properties*. Journal of Materials Chemistry C, **2013**, 1: p. 351.
16 Huang, Z.-M., Y. Z. Zhang, M. Kotaki and S. Ramakrishna, *A review on polymer nanofibers by electrospinning and their applications in nanocomposites*. Composites Science and Technology, **2003**, 63: p. 2223.
17 Lin, Q., Y. Li and M. Yang, *Polyaniline nanofiber humidity sensor prepared by electrospinning*. Sensors and Actuators B: Chemical, **2012**, 161: p. 967.
18 Ji, L., Z. Lin, Y. Li, S. Li, Y. Liang, O. Toprakci, Q. Shi and X. Zhang, *Formation and characterization of core-sheath nanofibers through electrospinning and surface-initiated polymerization*. Polymer, **2010**, 51: p. 4368.
19 Chronakis, I. S., S. Grapenson and A. Jakob, *Conductive polypyrrole nanofibers via electrospinning: Electrical and morphological properties*. Polymer, **2006**, 47: p. 1597.
20 Reneker, D. H. and A. L. Yarin, *Electrospinning jets and polymer nanofibers*. Polymer, **2008**, 49: p. 2387.
21 Norris, I. D., M. M. Shaker, F. K. Ko and A. G. MacDiarmid, *Electrostatic fabrication of ultrafine conducting fibers: polyaniline/polyethylene oxide blends*. Synthetic Metals, **2000**, 114: p. 109.
22 Bagheri, H. and A. Aghakhani, *Polyaniline-nylon-6 electrospun nanofibers for headspace adsorptive microextraction*. Anal Chim Acta, **2012**, 713: p. 63.
23 Sujith, K., A. M. Asha, P. Anjali, N. Sivakumar, K. R. V. Subramanian, S. V. Nair and A. Balakrishnan, *Fabrication of highly porous conducting PANI-C composite fiber mats via electrospinning*. Materials Letters, **2012**, 67: p. 376.
24 Aznar-Cervantes, S., M. I. Roca, J. G. Martinez, L. Meseguer-Olmo, J. L. Cenis, J. M. Moraleda and T. F. Otero, *Fabrication of conductive electrospun silk fibroin scaffolds by coating with polypyrrole for biomedical applications*. Bioelectrochemistry, **2012**, 85: p. 36.
25 Lee, J. Y., C. A. Bashur, A. S. Goldstein and C. E. Schmidt, *Polypyrrole-coated electrospun PLGA nanofibers for neural tissue applications*. Biomaterials, **2009**, 30: p. 4325.
26 Yu, Q.-Z., Z.-w. Dai and P. Lan, *Fabrication of high conductivity dual multi-porous poly (l-lactic acid)/polypyrrole composite micro/nanofiber film*. Materials Science and Engineering: B, **2011**, 176: p. 913.
27 Persano, L., C. Dagdeviren, Y. Su, Y. Zhang, S. Girardo, D. Pisignano, Y. Huang and J. A. Rogers, *High performance piezoelectric devices based on aligned arrays of nanofibers of poly(vinylidenefluoride-co-trifluoroethylene)*. Nat Commun, **2013**, 4: p. 1633.
28 Yang, Y., H. Zhang, G. Zhu, S. Lee, Z.-H. Lin and Z. L. Wang, *Flexible Hybrid Energy Cell for Simultaneously Harvesting Thermal, Mechanical, and Solar Energies*. ACS Nano, **2012**, 7: p. 785.
29 Chang, C., V. H. Tran, J. Wang, Y. K. Fuh and L. Lin, *Direct-write piezoelectric polymeric nanogenerator with high energy conversion efficiency*. Nano Lett, **2010**, 10: p. 726.
30 Dargahi, J., R. Sedaghati, H. Singh and S. Najarian, *Modeling and testing of an endoscopic piezoelectric-based tactile sensor*. Mechatronics, **2007**, 17: p. 462.
31 Shirinov, A. V. and W. K. Schomburg, *Pressure sensor from a PVDF film*. Sensors and Actuators A: Physical, **2008**, 142: p. 48.
32 Mičušík, M., M. Omastová, K. Boukerma, A. Albouy, M. M. Chehimi, M. Trchová and P. Fedorko, *Preparation, surface chemistry, and electrical conductivity of novel silicon carbide/polypyrrole composites containing an anionic surfactant*. Polymer Engineering & Science, **2007**, 47: p. 1198.
33 Merlini, C., A. R. dos Santos, M. A. D´Ávila, W. H. Schreiner and G. M. O. Barra, *Development of a Novel Pressure Sensing Material Based on Polypyrrole-Coated Electrospun Poly(vinylidene fluoride) fibers*. Materials Science and Engineering: B, **2013**, In Press: p.
34 Wu, N., Q. Cao, X. Wang and Q. Chen, *Study of a novel porous gel polymer electrolyte based on TPU/PVdF by electrospinning technique*. Solid State Ionics, **2011**, 203: p. 42.
35 Blinova, N. V., J. Stejskal, M. Trchová, J. Prokeš and M. Omastová, *Polyaniline and polypyrrole: A comparative study of the preparation*. European Polymer Journal, **2007**, 43: p. 2331.
36 Omastová, M., M. Trchová, J. Kovářová and J. Stejskal, *Synthesis and structural study of polypyrroles prepared in the presence of surfactants*. Synthetic Metals, **2003**, 138: p. 447.
37 Gregorio, R. and D. S. Borges, *Effect of crystallization rate on the formation of the polymorphs of solution cast poly(vinylidene fluoride)*. Polymer, **2008**, 49: p. 4009.
38 Kim, Y. J., C. H. Ahn, M. B. Lee and M. S. Choi, *Characteristics of electrospun PVDF/SiO2 composite nanofiber membranes as polymer electrolyte*. Materials Chemistry and Physics, **2011**, 127: p. 137.
39 Yu, L. and P. Cebe, *Crystal polymorphism in electrospun composite nanofibers of poly(vinylidene fluoride) with nanoclay*. Polymer, **2009**, 50: p. 2133.
40 Costa, L. M. M., R. E. S. Bretas and R. Gregorio Jr, *Effect of Solution Concentration on the Electrospray/Electrospinning Transition and on the Crystalline Phase of PVDF*. Materials Sciences and Applications, **2010**, 01: p. 246.

41 Cozza, E. S., O. Monticelli, E. Marsano and P. Cebe, *On the electrospinning of PVDF: influence of the experimental conditions on the nanofiber properties*. Polymer International, **2013**, 62: p. 41.
42 Zhong, Z., Q. Cao, B. Jing, X. Wang, X. Li and H. Deng, *Electrospun PVdF–PVC nanofibrous polymer electrolytes for polymer lithium-ion batteries*. Materials Science and Engineering: B, **2012**, 177: p. 86.
43 Leonard, C., J. L. Halary, L. Monnerie and F. Micheron, *DSC studies on the transitions in poly(vinylidenefluoride) and some related copolymers*. Polymer Bulletin, **1984**, 11: p. 195.
44 Loufakis, K. and B. Wunderlich, *Thermal analysis of the conformational disorder in semicrystalline poly(vinylidene fluoride) and poly(trifluoroethylene)*. Macromolecules, **1987**, 20: p. 2474.
45 Teyssedre, G., A. Bernes and C. Lacabanne, *Influence of the crystalline phase on the molecular mobiity of PVDF*. Journal of Polymer Science Part B-Polymer Physics, **1993**, 31: p. 2027.
46 Nabata, Y., *Molecular motion in form-II poly/vinylidene fluoride)*. Japanese Journal of Applied Physics Part 1-Regular Papers Short Notes & Review Papers, **1990**, 29: p. 2782.
47 Neidhofer, M., F. Beaume, L. Ibos, A. Bernes and C. Lacabanne, *Structural evolution of PVDF during storage or annealing*. Polymer, **2004**, 45: p. 1679.
48 Pramoda, K. P., A. Mohamed, I. Yee Phang and T. Liu, *Crystal transformation and thermomechanical properties of poly(vinylidene fluoride)/clay nanocomposites*. Polymer International, **2005**, 54: p. 226.
49 Lanceros-Méndez, S., J. F. Mano, A. M. Costa and V. H. Schmidt, *Ftir and Dsc Studies of Mechanically Deformed β-Pvdf Films*. Journal of Macromolecular Science, Part B, **2001**, 40: p. 517.
50 Chang, J., M. Dommer, C. Chang and L. Lin, *Piezoelectric nanofibers for energy scavenging applications*. Nano Energy, **2012**, 1: p. 356.
51 Sencadas, V., S. Lanceros-Méndez and J. F. Mano, *Characterization of poled and non-poled β-PVDF films using thermal analysis techniques*. Thermochimica Acta, **2004**, 424: p. 201.
52 Mano, J. F., V. Sencadas, A. M. Costa and S. Lanceros-Méndez, *Dynamic mechanical analysis and creep behaviour of β-PVDF films*. Materials Science and Engineering: A, **2004**, 370: p. 336.
53 Merlini, C., V. Soldi and G. M. O. Barra, *Influence of fiber surface treatment and length on physico-chemical properties of short random banana fiber-reinforced castor oil polyurethane composites*. Polymer Testing, **2011**, 30: p. 833.

